

# An Experimental Study on Rate Sensitivity of $J$ -Integral and its Evaluation by Small Punch Test for TRIP Steel

Leishi SHI<sup>1)</sup>, Takeshi IWAMOTO<sup>2)</sup>, Shinya HASHIMOTO<sup>3)</sup>

<sup>1)</sup> *Graduate School of Engineering, Hiroshima University*

1-4-1 Kagamiyama, Higashi-Hiroshima, Hiroshima, 739-8527 Japan  
e-mail: m124742@hiroshima-u.ac.jp

<sup>2)</sup> *Institute of Engineering, Hiroshima University*

1-4-1 Kagamiyama, Higashi-Hiroshima, Hiroshima, 739-8527 Japan

<sup>3)</sup> *SUZUKI Motor Corporation*

300 Takatsuka, Minami, Hamamatsu, 432-8611 Japan

Recently, much attention has been paid to TRIP steel since it indicates both high ductility and strength by strain induced martensitic transformation. This transformation allows TRIP steel to offer larger energy absorption than other steel at the same strength level. Therefore, it is expected to be applied to automobiles as security components that absorb energy upon collision. To produce the best performance of TRIP steel, the  $J$ -integral of TRIP steel should be investigated with respect to a various deformation rates for an evaluation of energy absorption. In the present study, the three point bending (3B) test is conducted for investigating the  $J$ -integral until the crack growth of TRIP steel. Then, in order to determine the energy absorption characteristic by the  $J$ -integral value at various locations in the components of TRIP steel, the size of the specimen should be very small. Thus, an SP test is introduced and conducted by using the newly established apparatus based on the SHPB method. By using the result of the SP test in conjunction with the result of a 3B test, the evaluation of the  $J$ -integral of TRIP steel subject to various deflection rates is attempted. The correlation between the  $J$ -integral and the equivalent fracture strain of the SP test for TRIP steel is challenged to be redefined.

**Key words:** TRIP steel, energy absorption,  $J$ -integral, rate sensitivity, small punch test, SHPB method.

## 1. INTRODUCTION

TRIP steel indicates high ductility, toughness and excellent energy absorption under plastic deformation by strain-induced martensitic transformation (SIMT) [1]. Recently, in order to improve passenger safety and reduce weight

of the car, the requirement of higher strength and excellent energy absorption of the steel used in the automobile industry has increased. Therefore, TRIP steel is expected to apply for the components which absorb energy upon collision.

Generally, the energy absorption is evaluated by calculating the area of the stress-strain curve obtained from the tensile test [2]. From this point of view, TOMITA and IWAMOTO [2] reported that energy absorption in TRIP steel decreases with an increase in strain rate. However, the dominant mechanism of those components for energy absorption is plastic-buckling with bending deformation. Due to a variety of impact velocity at the moment of the crash, the energy absorption characteristic of TRIP steel subjected to various rates of bending deflection becomes more important for a final product of the components. As RICE [3] defined, the  $J$ -integral can represent the total energy until the crack extension with its standardized experimental evaluation under the bending deformation. Over the past decade, the dynamic fracture toughness of steel is actively investigated [4] and a lot of investigations about the effect of rate sensitivity on mild steel have been done [5–7]; however, just a few studies on the fracture energy absorption sensitivity of the TRIP steel to the strain rate in experiment can be found [8, 9], especially under tension. In addition, just the clarification of its fracture energy absorption rate sensitivity for TRIP steel is insufficient. The residual stress and plastic strain in each location of the component are different, and SIMT will take place during the processing. In order to enhance and control the reliability and the performance of the product, the specimen picked out from the product should be very small to evaluate its characteristics.

In the past, several efforts have been made for the evaluation of energy absorption characteristics in metallic materials by the fracture parameters including the  $J$ -integral under static to dynamic loading based on the split Hopkinson pressure bar (SHPB) method [5, 10]. Especially, the fracture parameters of TRIP steel have been measured under quasi-static and impact tests [11, 12]. For studies by using the smaller specimen, a small punch (SP) test is well-employed to evaluate the  $J$ -integral [13–17]. By using this technique, the energy absorption for the part of the actual product of security components with respected to various deflection rate can be easily evaluated by a simple experiment. SHINDO *et al.* [14, 17] assessed the correlations between the equivalent fracture strain and the  $J$ -integral. In addition, they determined the  $J$ -integral in austenitic stainless steel, a kind of TRIP steel, and its weldment by combination between the SP test and FEA method. However, most of them are conducted under the low strain rate.

Due to the high impact velocity during the crash, it is important to clarify the energy absorption characteristic subjected to higher strain rate and its rate

sensitivity by evaluating the  $J$ -integral by an SP test. Additionally, RODRIGUEZ-MARTINEZ *et al.* [18] examined the behavior of AISI 304 steel sheets, which is a kind of TRIP steel, subjected to perforation under a wide range of impact velocities. The result shows the work hardening and ductility of AISI 304 are enhanced and the absorbing energy capability of AISI 304 is improved by SIMT during perforation. They are distinguishing the plastic deformation from the fracture characteristic for energy absorption. From the viewpoint of the SP test, it can be considered that the perforation can be connecting to the fracture characteristic.

In the present study, at first, the three-point bending (3B) test of pre-cracked specimen based on the ASTM standard is conducted for various deflection rates. Then, the  $J$ -integral associated with the crack growth is measured during a 3B test by the direct current potential difference method. After that, an impact SP apparatus base on the classical SHPB method is newly established. The load-deflection curves of SP test subject to various deflection rates are obtained by the conventional material testing machine, weight drop testing machine and the established SHPB apparatus, in conjunction with the results of the 3B test, evaluation of the energy absorption characteristic of TRIP steel by the  $J$ -integral is attempted. The relationship between the  $J$ -integral and the equivalent fracture strain of the SP test is challenged to be redefined for various deflection rates. Finally, a rate sensitivity of energy absorption in TRIP steel is discussed.

## 2. THREE POINT BENDING TEST (3B)

### 2.1. Method of three point bending test (3B)

In order to evaluate the  $J$ -integral before crack initiation, it is essential to find the point of the crack initiation on the load-deflection curve. Therefore, in this investigation, a direct current potential difference (DCPD) technique is introduced.

The DCPD method is one of the most accurate and efficient methods for monitoring the crack initiation and propagation in real time during deformation. By applying current to the specimen, the electrical potential difference between the crack faces is generated. A crack initiation is considered to be coincident with a sudden increase in potential difference. As the crack initiates, the resistance will be increased. This leads to an increased potential difference. As shown in Fig. 1. The load-time and voltage-time curve can be recorded and the moment when the voltage suddenly increased is defined as the point of crack initiation [19].

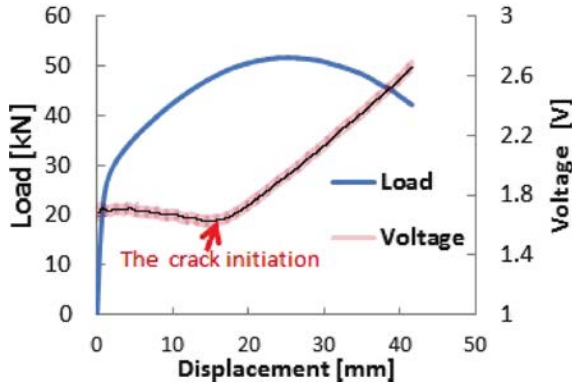


FIG. 1. An example of a result obtained by the DCPD method to determine the point of crack initiation.

2.2. Samples used for 3B test

Pre-cracked specimens made of AISI304, a kind of TRIP steel, are used in this test. The dimensions of the pre-cracked specimen follow the ASTM standard as shown in Fig. 2. To get an austenitic structure, the specimen is subjected to solution heat treatment at 1323K for 30 min by electric furnaces and then quenched in water.

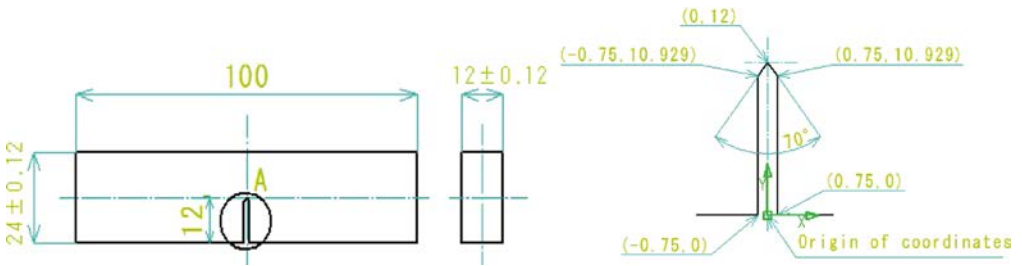


FIG. 2. The dimensions of the specimen for 3B test.

2.3. Measurement apparatus of 3B test

Figure 3 shows the schematic diagram of the locations of probes for measuring voltage and supplying current. Two probes that are independent of the current supplement are used to measure the voltage. The circuit is based on the four-probe method for precise measurement of voltages. In order to make the probes as sensitive as possible, they are fixed around the pre-crack on the opposite side in the thickness direction of the specimen. The current supplied wire and the probes for measuring the voltage are spot-welded to the specimen. The current is set as 12 A.

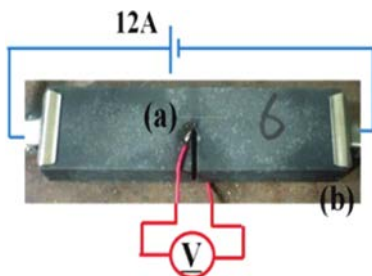


FIG. 3. A photograph of the specimen with some drawings of the circuit to show locations of the probes for measuring voltage and supplying current.

In the quasi-static test, the signal from the signal conditioner (Kyowa CDV-700A) for recording the potential difference is put into the conventional material testing machine (Shimadzu AG-250kNXplus), which is shown in Fig. 4. The speeds of crosshead are set as 0.2, 2, 20 and 200 mm/min. The relationship of load-displacement and potential-difference-displacement are recorded simultaneously.

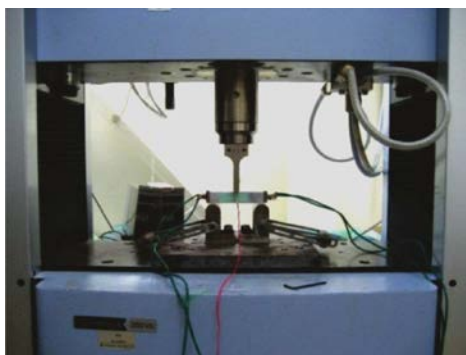


FIG. 4. The photograph of the quasi-static three-point bending test apparatus.

Figure 5 shows the schematic illustration and a photograph of the drop weight testing setup. In this test, the load and potential difference are recorded by the oscilloscope (Yokogawa DL-2700) at the same time. A load sensing block [20] which can capture the load and protect the reflected wave propagates back into the load sensing part set just under the center. Figure 6 shows a photograph of the load sensing block used in the present study. The load sensing block has a small projection. Two strain gauges are glued axisymmetrically at the middle of the projection. These two strain gauges are connected to a digital oscilloscope (Yokogawa DL-2700) via a signal conditioner (Kyowa CDV-700A) for amplifying the voltage signal. According to the relationship between voltage and load calibrated by using the material testing machine, a voltage-time curve can be transform into a load-time curve. Weight is dropped from a height of

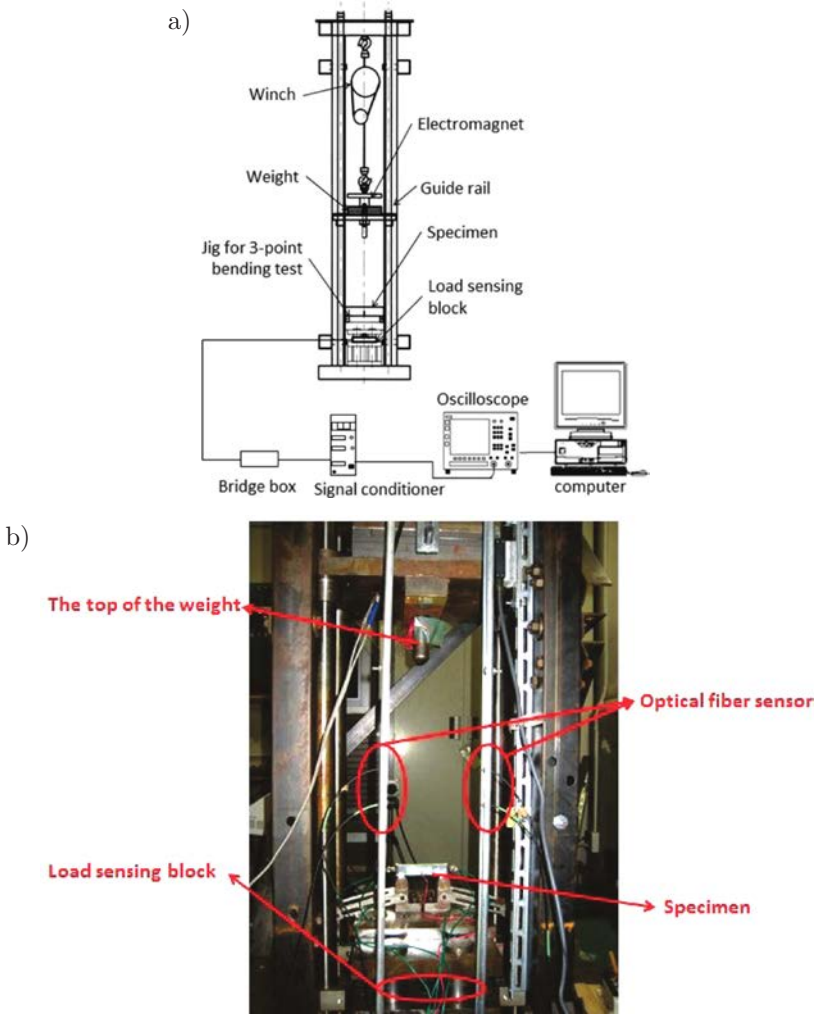


FIG. 5. a) A schematic and b) a photograph of the drop weight test setup.

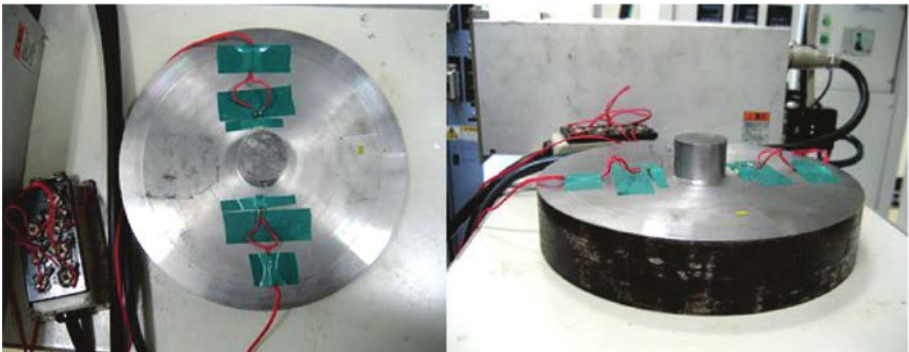


FIG. 6. The photograph of the load sensing block used in drop weight test.

700 mm and 900 mm respectively. The deflection with respect to time is recorded by a high speed camera during impact. The deflection rate can be calculated from a deflection-time curve by the finite difference method. The corresponding deflection rates in the impact are approximately 3190 mm/s and 3530 mm/s. The normalized deflection rates can be calculated as  $40 \text{ s}^{-1}$  and  $45 \text{ s}^{-1}$  divided by the span length of 80 mm, respectively.

#### 2.4. The manner of data processing

In this investigation the simple formula for evaluating the  $J$ -integral under bending deformation derived by RICE [21] is used. The formula is given by the following equation.

$$(2.1) \quad J = \frac{Af(a_0/W)}{B(W-a)},$$

where  $A$  is the area under the load-deflection curve up to the point of crack initiation. It can be calculated by using the DCPD method as described in Subsec. 2.1.  $B$  and  $W$  are the initial thickness and width of the specimen respectively.  $a$  is the initial crack length including the notch and the fatigue pre-crack. Since the aim of this investigation is to evaluate the energy absorption characteristic of TRIP steel with an extremely high ductility. The dimensions of the specimen are based on the ASTM standard. Therefore  $a$  is equal to 14.4 mm and a value of two for  $f(a_0/W)$  is employed.

#### 2.5. Discussion on the result of 3B test

Figure 7 shows the relationship between the  $J$ -integral and the normalized deflection obtained from the 3B test. It presents an approximately linear rela-

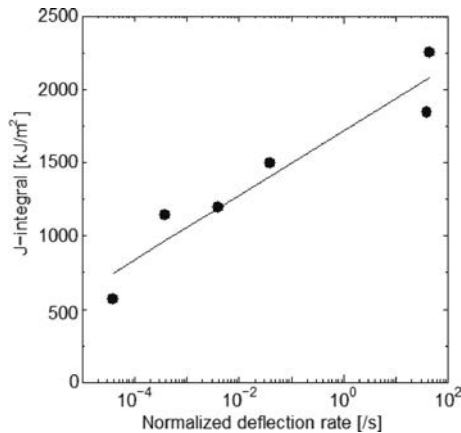


FIG. 7. Relationship between the  $J$ -integral and the normalized deflection rate of 3B test.

tionship between the  $J$ -integral and the normalized deflection rate on the semi-logarithmic plot. A positive rate-sensitivity can be observed by the  $J$ -integral value's increase with an increase in the deflection rate.

### 3. SMALL PUNCH TEST

#### 3.1. Samples used for small punch test

Two kinds of material are employed in this test, aluminum alloy 6061 and AISI304. The aluminum alloy specimen is used for confirming the validity of the established apparatus for SP test under quasi-static test. Both of them are machined to a disk shape and they both have dimensions of 10 mm in diameter and 0.5 mm in thickness. The specimen, made of AISI304, is subjected to solution heat treatment at 1323K for 30 minutes by electric furnaces and then quenched in water.

#### 3.2. Measurement apparatus

3.2.1. *The SP test apparatus for quasi-static SP test.* Figure 8 shows the established apparatus for the quasi-static SP test and the schematic figure of jigs for both quasi-static and drop weight SP test. It consists of upper and lower dies, four clamping screws and a puncher. In order to keep the centers of the punch, specimen and dies in as a straight a line as possible, a cylindrical collar is employed here. In order to prevent the specimen being subjected to frictional

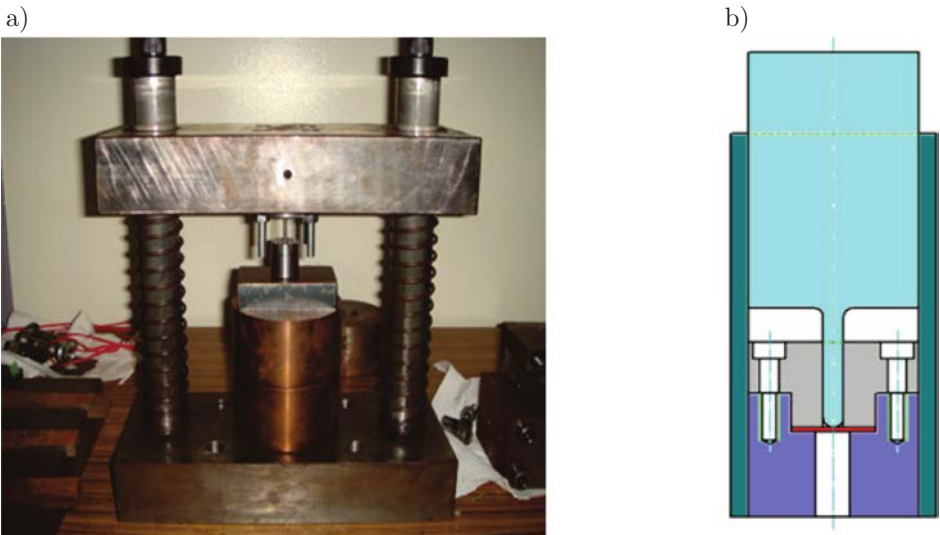


FIG. 8. a) The established apparatus for the quasi-static SP test and b) a schematic of jigs for both quasi-static and drop weight SP test.

forces during deformation, the bore diameter in the lower dies is determined as follows [22]

$$(3.1) \quad d_2 \geq d_1 + 2t_0,$$

where  $d_1$ ,  $d_2$  and  $t_0$  are the outer diameter of the lower die, the inner diameter of the upper die and the original thickness of the specimen respectively. In present study,  $d_1$  is decided as 2.4 mm and  $d_2$  is decided as 4 mm.

The quasi-static test is conducted with a conventional material testing machine, and the crosshead speeds are set as 0.2, 2, 20 and 200 mm/min.

*3.2.2. Confirm the validity of the apparatus.* In order to confirm the validity of the apparatus which was established for SP test, the SP test is conducted by the same setup and condition with past research work [16]. Figure 9 shows the comparison of the load-deflection curves under quasi-static test obtained by the present study and the previous study. The result of the present study coincide with the previous study, and so, we can find that the apparatus manufactured here is valid.

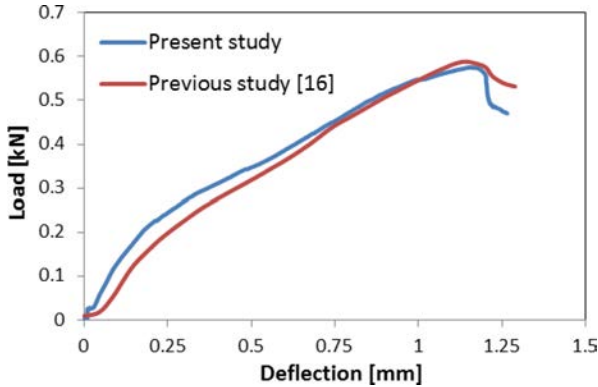


FIG. 9. The comparison of the load-deflection curves obtained by the present study and a previous study [16].

*3.2.3. The SP test apparatus based on the drop weight method.* The jig for SP test based on the drop weight method is shown in Fig. 10. The SP test apparatus is placed on the center of the steel plate. Weight is dropped from a height of 20 mm. The speed of the weight at the moment of impact can be calculated by using two optical fiber sensors. A gauge line is marked on the top of the puncher. By tracking the position of the gauge line with the high speed camera, the displacement with respect to the time of the punch can be obtained as shown in Fig. 11a. The load during the impact can be recorded by the load sensor block which is as same as the drop weight 3B test is shown in Fig. 11b.

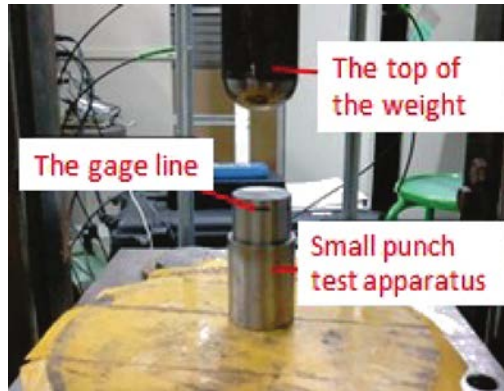


FIG. 10. The jig used for SP test based on the drop weight test method.

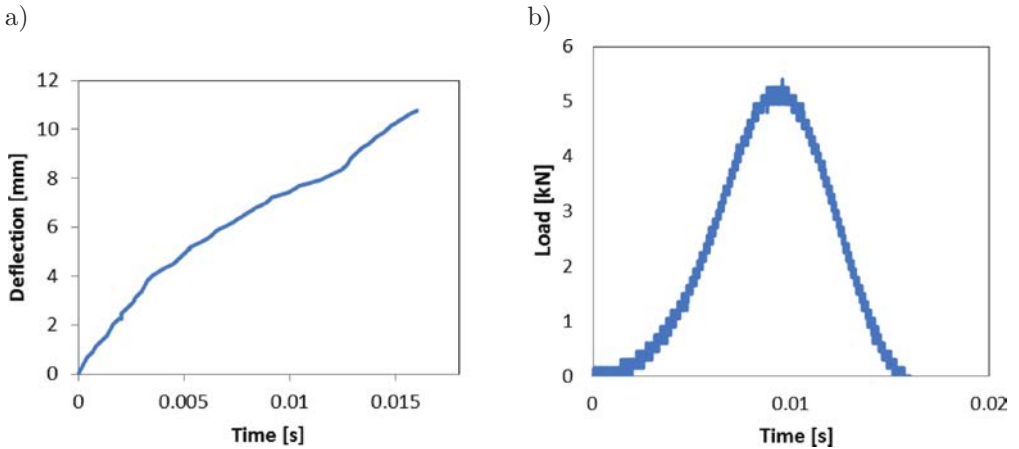
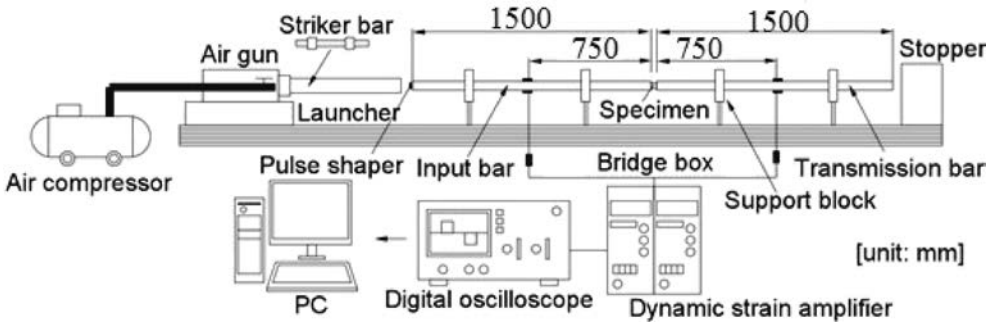


FIG. 11. The deflection-time curve (a) and load-time curve (b) obtained by SP test based on drop weight test method.

*3.2.4. The impact SP test based on SHPB method.* To conduct the impact SP test under high loading speed, an impact SP test apparatus is newly established based on the SHPB method. The schematic picture of the established apparatus is shown in Fig. 12. It consists of an air gun, a striker bar, an input bar, an output tube and some measurement devices. The puncher and the lower die are directly manufactured at the ends of the input bar and the output tube respectively. The upper die is connected to lower die with the output tube by a thread and the specimen is clamped between the upper die and the output tube. A collar with lower mechanical impedance is used to keep straightness of the center of the punch and the specimen. The dimensions of this apparatus are also designed by Eq. (3.1). When the air gun launches the striker bar to impact

on the edge of input bar by a sudden release of compressed air, a stress pulse is generated and propagated along the input bar toward the specimen. After it arrived the specimen, partially of it reflected back into the input bar as the reflected strain pulse, and the residual pulse transmitted through the specimen into the output bar as the transmitted strain pulse. To record the strain wave in the pressure bar and tube, the semi-conductor strain gauges (Kyowa KSP-z-120-E4) are glued axisymmetrically at the middle of the pressure bar and tube. All strain gages are connected to a digital oscilloscope (Yokogawa DL-2700) via signal conditioner (Kyowa CDV-700A) for amplifying the voltage signal.

a)



b)

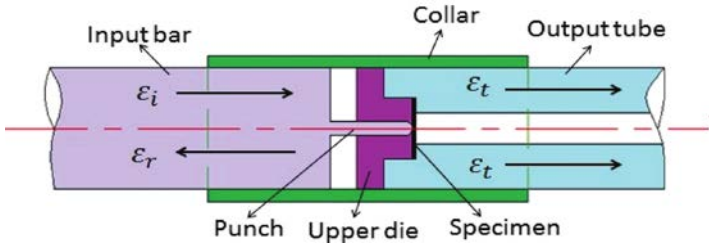


FIG. 12. The schematic picture of the established apparatus for the SP test based on SHPB method: a) whole of the apparatus; b) near the specimen including upper die and collar.

The stress pulses propagating through the incident and transmitter bars,  $\sigma_i$ ,  $\sigma_r$ ,  $\sigma_t$  can be obtained respectively. Obeying the one-dimensional elastic wave propagation theory, particle velocities in the incident and transmitter bars  $v_{in}$  and  $v_{out}$  can be obtained by the following equation.

$$(3.2) \quad v_{inp}(t) = \frac{\sigma_i(t) - \sigma_r(t)}{\rho c},$$

$$v_{out}(t) = \frac{\sigma_t(t)}{\rho c},$$

where  $\rho$  and  $c$  are mass density and velocity of longitudinal elastic wave in pressure bars. Using the following equation, a deflection at the center of the specimen  $\delta(t)$  is calculated as

$$(3.3) \quad \delta(t) = \int_0^t \{v_{\text{inp}}(t) - v_{\text{out}}(t)\} dt'.$$

According to results above, the input load  $P_{\text{inp}}(t)$  and load at support point  $P_{\text{sup}}(t)$  can be calculated by the follow equation:

$$(3.4) \quad P_{\text{inp}}(t) = [\sigma_i(t) + \sigma_r(t)] A_{\text{in}}, \quad P_{\text{sup}}(t) = \sigma_t(t) A_{\text{out}},$$

where  $A_{\text{in}}$  is the cross-sectional area of the input bar and  $A_{\text{out}}$  is the cross-sectional area of the output bar. In general, the stress wave obtained by SHPB method has the initial oscillation. To reduce the initial oscillation, the pulse shaper technique was introduced [23, 24].

### 3.3. The manner of data processing

In the present study, the  $J$ -integral is calculated by using the method proposed by SHINDO *et al.* [17]. The determination process of the evaluation equation is given as follows.

At first, the equivalent fracture strain, which is very important in order to obtain the  $J$ -integral of the SP test, is derived by using the follow equation under the assumption of constant volume during plastic deformation:

$$(3.5) \quad \bar{\varepsilon}_{qf} = \ln\left(\frac{t_0}{t}\right),$$

where  $t_0$  is the initial thickness of specimen and  $t$  is the thickness of the fracture part measured after the experiment. In the present study,  $t_0$  is equal to 0.5 mm and  $t$  in the part of the fracture on the specimen is measured by using a micrometer. The plotted relationship between  $\ln(\ln(t_0/t))$  and  $\ln(\delta_{\text{max}}/t_0)$  have an approximate linear relationship. Therefore, we can obtain the following equation,

$$(3.6) \quad \bar{\varepsilon}_{qf} = \alpha \left(\frac{\delta_{\text{max}}}{t_0}\right)^n,$$

where  $t_0$  is the initial thickness of specimen,  $\delta_{\text{max}}$  is the deflection at the maximum load obtained by the load-deflection curve from the SP test. From the correlation between  $\ln(\ln(t_0/t))$  and  $\ln(\delta_{\text{max}}/t_0)$ ,  $\alpha$  and  $n$  can be identified. Then

according to the method by SHINDO *et al.* [17], the  $J$ -integral obtained by experimental results of the  $J$ -integral using CT specimen has an approximate linear relationship with equivalent fracture strain which obtained by SP test at same deflection rate. The linear equation can be obtained as follows:

$$(3.7) \quad J_{in} = A\bar{\epsilon}_{qf} - B,$$

where  $A$  and  $B$  are parameters, respectively.

### 3.4. Discussion on the result of SP test

Figure 13 shows the load-deflection curve at the various deflection rate obtained by the SP test. As shown in this figure, the deflection at the maximum load increases with an increasing deflection rate. Generally, in the conventional tensile test for the metallic material, the load increases with an increase of strain rates. At the same time, the maximum strain for failure becomes lower with an increase of the strain rate. This implies that the strength becomes larger, but the ductility decreases with respect to the strain rate. However, in the present study an opposite tendency on the rate sensitivity of the deflection is observed.

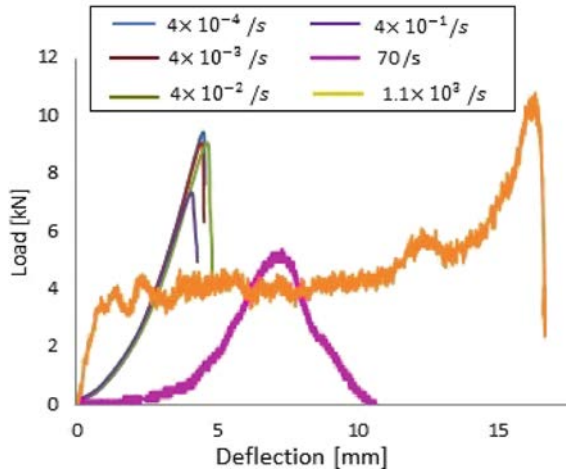


FIG. 13. Load-deflection curves at various deflection rates.

Figure 14 shows the stress waves captured from the impact SP test based on the SHPB method. Here it is observed that transmitted wave is quite small compared with the incident and reflected waves. This phenomenon may be caused by the stress wave becoming quite small when it is transmitted to the output tube. Since the cross-section area may be large relative to the cross-section area of the punch, most of the stress wave is reflected when the punch hits the specimen

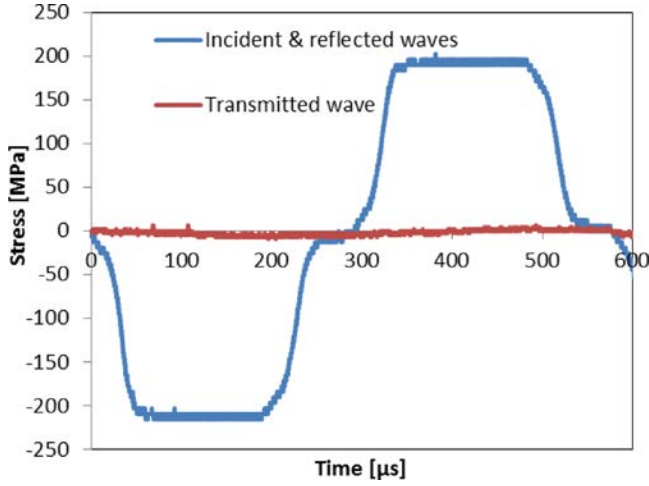


FIG. 14. Incident, reflected and transmitted pulse obtained from impact small punch testing.

and the load turn to smaller. In addition, the friction between the punch and the specimen maybe created during the impact. It leads a partial of incident stress consumed during the fracture process. However, the load and deflection still can be calculated because the signal itself can be captured by an appropriate adjustment of the resolution in output voltage.

#### 4. DISCUSSION ON THE RESULT OF THE WHOLE WORK

Following the steps described in the Subsec. 3.3, the approximately linear relationship between  $\ln(\ln(t_0/t))$  and  $\ln(\delta_{\max}/t_0)$ , and the relation between the  $J$ -integral and fracture strain can be obtained as shown in Fig. 15 and the parameters of Eq. (3.6) and Eq. (3.7) are identified by these two relationship. The final equations are shown as follow.

$$(4.1) \quad \bar{\epsilon}_{qf} = 0.001 \left( \frac{\delta_{\max}}{t_0} \right)^{2.54},$$

$$(4.2) \quad J = 1970\bar{\epsilon}_{qf} + 633.$$

Unfortunately, as shown in Fig. 15b, it is hard to describe the corresponding  $J$ -integral for the result of the SP test based on the SHPB method. However, the maximum load of the SP test based on the SHPB method is known. Therefore, it is allowed that the  $J$ -integral at such higher deflection rate can be calculated by using above two equations and it becomes approximately 7922 kJ/m<sup>2</sup>. Nevertheless, according to the approximate linear relationship which obtained

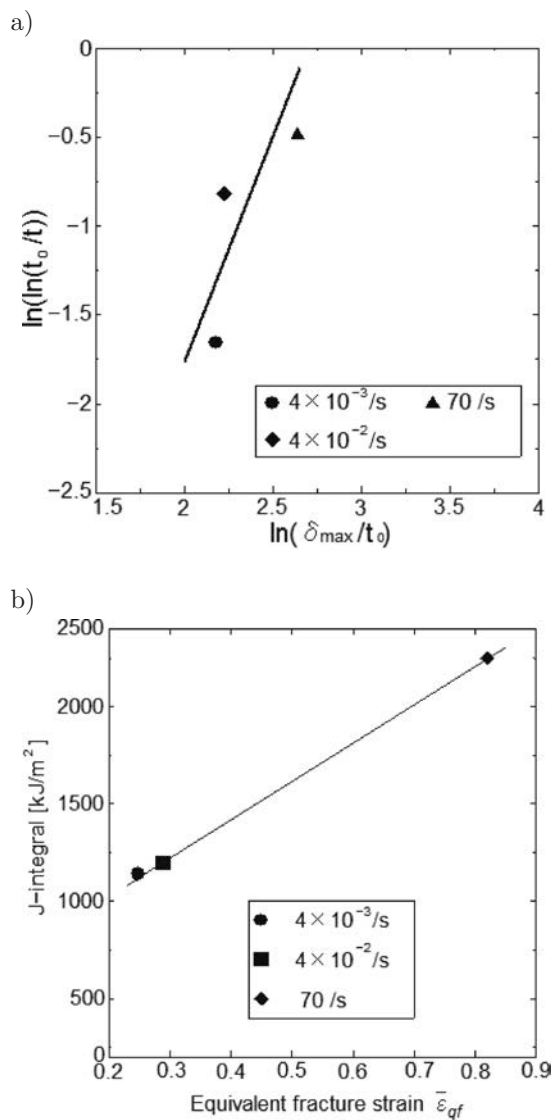


FIG. 15. a) The approximately linear relationship between  $\ln(\ln(t/t_0))$  and  $\ln(\delta_{\max}/t_0)$ ,  
 b) the relation between the  $J$ -integral and equivalent fracture strain.

from Fig. 7, the  $J$ -integral of 3B test base on SHPB method should be approximately  $2456 \text{ kJ}/\text{m}^2$ . Therefore, we can conject that the  $J$ -integral may be not have a linear relationship with normalized deflection rate under high strain rates anymore. This means that a different mechanism for energy absorption occurs in the range of higher deflection rate compared with the result of the 3B test by the drop weight machine.

In the previous study [17], the parameters for the Eq. (3.6) and Eq. (3.7) have been identified for austenitic stainless steel at the cryogenic temperature. Here, in order to compare this with the relations defined by the previous study [17], the  $J$ -integral is calculated using their parameters and  $\delta_{\max}$  of the results in present study. The result is shown in Fig. 16. Compare with the result shown in Fig. 7 the values of  $J$ -integral are approximately four times the results obtained by 3B test at the same deflection rate. Taking into consideration that the equations by SHINDO *et al.* [17] are defined at the cryogenic temperature, the  $J$ -integral value maybe overestimated.

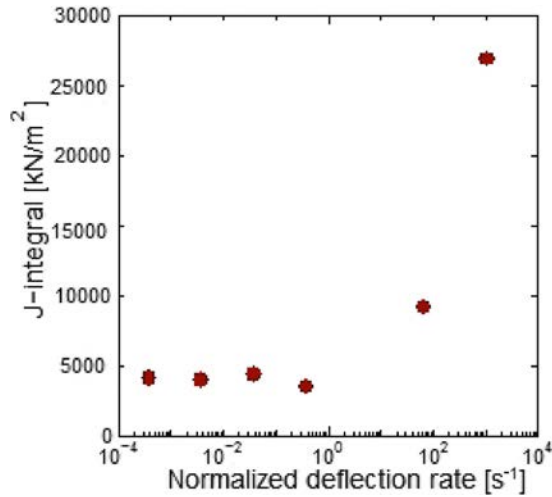


FIG. 16. The relationship between the  $J$ -integral and normalized deflection rate.

In the present study, a relationship between the energy absorption characteristic up to crack initiation and the normalized deflection rate was obtained by  $J$ -integral. The apparatus for impact SP test based on the modified SPBH method was established. By using the result of the 3B test, the relation between  $J$ -integral and the equivalent fracture strain under the SP test was redefined. Finally, the fracture energy absorption of SP test obtained by SHPB method was calculated. An experimental method for studying the rate sensitivity of energy absorption was established.

#### ACKNOWLEDGMENT

We gratefully acknowledge financial supports from a Grant-in-Aid for Scientific Research from the Ministry of Education, Culture, Sports, Science and Technology, Japan.

## REFERENCES

1. ZACKAY V.F., PARKER E.R., FAHR D., BUSCH R., *The enhancement of ductility in high-strength steels*, Trans. ASM, Quart., **60**, 252–259, 1967.
2. TOMITA Y., IWAMOTO T., *Constitutive modeling of TRIP steel and its application to the improvement of mechanical properties*, Int. J. Mech. Sci., **37**, 12, 1295–1305, 1995.
3. RICE J.R., *A path independent integral and the approximate analysis of strain concentration by notches and cracks*, J. App. Mech., **35**, 379–386, 1968.
4. KOBAYASHI T., YAMAMOTO I., NIINOMI M., *Evaluation of the dynamic fracture toughness parameters by instrumented charpy test* [in Japanese], Tetsu-to-Hagane, **16**, 1934–1940, 1985.
5. KLEPACZKO J.R., *Discussion of a new experimental method in measuring fracture toughness initiation at high loading rates by stress waves*, J. Eng. Mater. Technol., Trans. of ASM, **104**, 1, 29–35, 1982.
6. XU Z., LI Y., *Study of loading rate effect on dynamic fracture toughness of high strength steel under impact loading*, Streng. Fract. Compl., **6**, 1–2, 17–23, 2010.
7. KALTHOFF J.F., *Fracture behavior under high rates of loading*, Eng. Fract. Mech., **23**, 1, 289–298, 1986.
8. BLECK W., SCHAEEL I., *Determination of crash-relevant material parameters by dynamic tensile tests*, Steel Research, **71**, 173–178, 2000.
9. CHOI I.D., BRUCE D.M., KIM S.J., LEE C.G., PARK S.H., MATLOCK D.K., SPEER J.G., *Deformation Behavior of Low Carbon TRIP Sheet Steels at High Strain Rates*, ISIJ Int. J., **42**, 12, 1483–1489, 2002.
10. YOKOYAMA T., KISHIDA K., *A novel impact three-point bend test method for determining dynamic fracture-initiation toughness*, Exp. Mech., **29**, 2, 188–194, 1989.
11. KOBAYASHI T., WAKAI N., YAGI W., KAZINO T., UEDA Y., *Effects of manganese and nickel increase on mechanical properties of TRIP Steel* [in Japanese], Tetsu-to-Hagane, **71**, 9, 1178–1185, 1985.
12. ANTOLOVICH S.D., SINGH B., *On the toughness increment associated with the austenite to martensite phase transformation in TRIP steels*, Metall. Mater. Trans. B, **2**, 8, 2135–2141, 1971
13. MAO X., TAKAHASHI H., *Development of a further-miniaturized specimen of 3 mm diameter for tem disk small punch tests*, J. Nucl. Mater., **150**, 1, 42–52, 1987.
14. SHINDO Y., YAMAGUCHI Y., HORIGUCHI K., *Small punch testing for determining the cryogenic fracture properties of 304 and 316 austenitic stainless steels in a high magnetic field*, Cryogenics, **44**, 11, 789–792, 2004.
15. FOULDS J., VISWANATHAN R., *Small Punch Testing for Determining the Material Toughness of Low Alloy Steel Components in Service*, J. Eng. Mater. Technol., **116**, 4, 457–464, 1994.
16. BUDZAKOSKA E., CARR D.G., STATHERS P.A., LI H., HARRISON R.P., HELLIER A.K., YEUNG W.Y., *Predicting the Jintegral fracture toughness of Al 6061 using the small punch test*, Fat. Fract. Eng. Mater. Struct., **30**, 9, 796–807, 2007.

17. SHINDO Y., HORIGUCHI K., SUGO T., MANO Y., *Finite element analysis and small punch testing for determining the cryogenic fracture toughness of austenitic stainless steel weld*, J. Test. Eval., **28**, 6, 431–437, 2000.
18. RODRIGUEZ-MARTINEZ J.A., RUSINEK A., PESCI R., *Experimental survey on the behaviour of SISI 304 steel sheets subjected to perforation*, Thin-Walled Struct., **48**, 12, 966–978, 2010.
19. BROWN W.F., SRAWLEY J.E., *Fracture toughness testing*, ASTM Spec. Tech Publ., **381**, 175–180, 1965
20. CHUMAN Y., MIMURA K., KAIZU K., TANIMURA S., *A sensing block method for measuring impact force generated at a contact part*, Int. J. Impact Eng., **19**, 2, 165–174, 1997.
21. RICE J.R., PARIS P.C., MERKLE J.G., *Some further results of J-Integral analysis and estimates*, ASTM STP536, 231–245, 1973.
22. MAO X., TAKAHASHI H., *Development of a further-miniaturized specimen of 3 mm diameter for TEM disk small punch tests*, J. Nuclear Materials, **150**, 42–52, 1987.
23. NEMAT-NASSER S., ISAACS J.B., STARRETT J.E., *Hopkinson Techniques for Dynamic Recovery Experiments*, Proc. Roy. Soc. Lond., A, **435**, 1894, 371–391, 1991.
24. FREW D.J., FORRESTAL M.J., CHEN W., *Pulse Shaping Techniques for Testing Elastic-plastic Materials with a Split Hopkinson Pressure Bar*, Exp. Mech., **45**, 2, 186–195, 2005.

*Received November 12, 2012; revised version March 5, 2013.*

---